Ambient protection of black phosphorus via sequestration of reactive oxygen species

Sumeet Walia[1]*, Sivacarendran Balendhran[1], Taimur Ahmed[1], Mandeep Singh[2], Christopher El-Badawi[3], Mathew D. Brennan[4], Pabudi Weerathunge[2], Md. Nurul Karim[2], Fahmida Rahman[1], Andrea Rassell[5], Jonathan Duckworth[5], Rajesh Ramanathan[2], Gavin E. Collis[6], Charlene J. Lobo[3], Milos Toth[3], Jimmy Christopher Kotsakidis[7], Bent Weber[7], Michael Fuhrer[7], Jose Manuel Dominguez-Vera[8], Michelle J. S. Spencer[4], Igor Aharonovich[3], Sharath Sriram[1], Madhu Bhaskaran[1] and Vipul Bansal[2]*

[1]Functional Materials and Microsystems Research Group, School of Engineering, RMIT University, Melbourne 3000, Victoria, Australia

[2]Ian Potter NanoBioSensing Facility, NanoBiotechnology Research Laboratory, School of Science, RMIT University, Melbourne 3000, Victoria, Australia

[3]School of Mathematical and Physical Sciences, University of Technology Sydney, Ultimo 2007, NSW, Australia

[4]School of Science, RMIT University, Melbourne 3001, Victoria, Australia

[5]School of Media and Communication, RMIT University, Melbourne 3000, Victoria, Australia

[6]CSIRO Manufacturing, CSIRO, Bayview Avenue, Clayton 3168, Victoria, Australia

[7]School of Physics and Monash Centre for Atomically Thin Materials, Monash University, Clayton 3800, Victoria, Australia

[8]Departamento de Qu´ımica Inorganica, Facultad de Ciencias, Universidad de Granada, E-18071, Granada, Spain

Black phosphorous (BP) has recently emerged as a promising candidate for next generation of nanophotonic and nanoeletronic devices. However, rapid ambient degradation of mechanically exfoliated BP poses challenges in its practical deployment in scalable devices.[1] To date, the strategies employed to protect BP have relied upon preventing its exposure to atmospheric conditions.[2, 3] Here we report an approach that allows this sensitive material to remain stable without requiring its isolation from the ambient environment. Our method draws inspiration from the unique ability of biological systems to avoid photo-oxidative damage caused by reactive oxygen species (ROS).[3] Since BP undergoes similar photo-oxidative degradation,[4] we employ imidazolium-based room temperature ionic liquids (RTILs) as quenchers of these damaging species. This chemical sequestration strategy allows BP to remain stable for over thirteen weeks, while retaining its key electronic characteristics. This study opens opportunities to practically implement BP and other environmentally-sensitive two dimensional (2D) materials for opto-electronic applications.

The tunable intrinsic bandgap (~0.3 eV for bulk and ~2 eV for monolayer)[5, 6], high carrier mobility and highly anisotropic properties of BP,[5, 7-9] make it a desirable candidate for a variety of applications, including energy generation and storage systems as well as chemical/bio-sensing.[10-13] For most of these applications, the material does not necessarily need to be in the form of a monolayer, but rather as a thin film, composite, or an embedded structure.[14]

A fundamental challenge hampering implementation of few-layer BP in practical devices is its vulnerability to ambient degradation within a few hours.[15, 16] As a result the material rapidly loses its semiconducting properties and is rendered unusable. The mechanism and causes of this degradation is still a subject of investigation, with recent reports indicating the combination of light and oxygen in the presence of ambient moisture being the key factor. Assuming these factors play a synergistic role, analogies may be drawn between the BP degradation mechanism and biological systems. An elegant example is photosystem II chemistry in plants, wherein a combination of light

and oxygen is known to produce highly oxidising radicals and ROS that are toxic to organisms.[17] However, the biological systems have the unique ability to protect and/or repair themselves from such photo-oxidative damages by employing a number of antioxidants.[17]

Chemical modifications have been widely utilised to manipulate the optical and electronic properties of nanomaterials.[18-24] However, these approaches have not utilised the antioxidant potential of molecules that could actually sequester the damaging ROS generated on the nanomaterial surface through environmental interactions, which eventually causes material degradation.

In this work, we carefully engineer a scalable biomimetic platform to protect environmentally-sensitive 2D materials through their surface treatment with antioxidant molecules. In particular, we exploit the ROS quenching ability of RTILs to stabilise few-layer BP against ambient oxidation. We choose two imidazolium based RTILs, with the same 1-Butyl-3-methylimidazolium [BMIM] cation, but with different anions. Tetrafluoroborate [BF_4] anion makes the RTIL highly polar, whereas hexafluorophosphate [PF_6] anion makes the RTIL non-polar. Our investigations begin with the hypothesis that the hydrophobicity of [BMIM][PF_6] may be more favourable in providing resistance against BP degradation, since ambient moisture is known to facilitate photo-oxidation of BP.[Ref] We treat the surface of two separate BP flakes using these two RTILs and test their effectiveness using an *in situ* environmental scanning electron microscopy (ESEM) technique. ESEM is used both to simulate the oxidising chemical reactions that degrade BP, and to monitor the degradation rate in real time (Fig. 1). This is achieved simply by imaging BP using an electron beam whilst the ESEM vacuum chamber is filled with a small amount (~ 8 Pa) of H_2O vapour.

Electron irradiation under such conditions is known to generate highly reactive radicals that give rise to oxidation in the vicinity of the electron beam, thereby leading to chemical etching of even the strongest and most inert materials such as diamond.[25] Figure 1a shows a schematic

representation of this process. Here, the radicals give rise to the rapid degradation of pristine BP within 15 min of imaging (corresponding to an electron irradiation fluence of 2.71×10^{19} electrons cm^{-2}) as seen in Fig. 1b and Supplementary Video 1. In contrast, the RTIL-treated samples are significantly more resilient and able to withstand more aggressive electron exposures. The [BMIM][PF_6]-treated BP deteriorates only partially after 120 min of electron exposure (corresponding to an electron fluence of 5.43×10^{21} electrons cm^{-2}), as is seen in Fig. 1c and Supplementary Video 2. The [BMIM][BF_4]-treated BP is highly stable and resilient even after 180 min of exposure and a total electron beam fluence of 1.58×10^{22} electrons cm^{-2} (see Fig. 1d and Supplementary Video 3). To confirm that the BP degradation seen in the ESEM images is caused by radicals generated through the dissociation of H_2O rather than by direct electron beam damage, reference exposures were performed in high vacuum (~3×10^{-4} Pa), where the observed degradation rate is several orders of magnitude lower than in the presence of 8 Pa of H_2O vapor (see Supplementary Fig. S1). Hence, our *in situ* ESEM studies validate the dominant role of ROS in BP degradation, while establishing that the relative hydrophobicity of [BMIM][PF_6] (shown in Fig. 1b) does not result in superior stabilisation of BP.

To obtain insights into the nature of binding of RTILs to BP, we performed density functional theory (DFT) calculations (Fig. 2). The modelling studies for both basal and edge planes of monolayer BP reveal that in the presence of the [BF_4] anion, the [BMIM] cation binds more strongly to BP, than in the presence of the [PF_6] anion (other optimised structures are shown in supplementary information, Fig. S2-S7). As BP degradation is observed to initiate from its edge plane, we also modelled the influence of the crowding effect of RTILs at the BP edge. Introduction of additional molecule makes RTIL binding to BP more favourable without influencing the relative binding affinity of the two RTILs towards BP. It is noted that even though in the case of both RTILs, the chemisorption of [BMIM] cation to BP through its imidazole ring is thermodynamically favoured; the electrostatic interactions between the anion and the cation play an important role in

dictating the final binding energies. Further, the binding of the RTILs to BP appear to cause lattice distortions, similar to those observed previously, when aryl diazonium chemistry was explored for surface passivation of exfoliated BP.[23] The binding of RTILs to BP is experimentally validated by atomic force microscopy (AFM) that reveals an increase in the surface roughness of the flakes (see Supplementary Fig. S8). As such, theoretical and experimental studies collectively reveal that stronger binding of [BMIM][BF_4] to BP makes it a superior stabilising agent compared to [BMIM][PF_6]. As a result, we further focus our investigations on studying the role of this particular RTIL (i.e. [BMIM][BF_4]) in BP stabilisation and its use in practical devices.

We employ X-ray photoelectron spectroscopy (XPS) to study the binding of [BMIM][BF_4] to the BP surface and its effect on stabilisation. The chemical nature of surface-treated BP was probed with C 1*s*, N 1*s*, and P 2*p* core level XPS spectra. The P 2*p* core level binding energies show features corresponding to P-P (130 eV), P-C (132.5 eV), P-N (133.5 eV) and P-O (134.1 eV), which agree well with literature assignments (Fig. 3a).[23, 26] The P-C (284 eV)[23] and P-N (401.1 eV) signatures are also observed in the C 1*s* and N 1*s* spectra, supporting the chemisorption of the imidazolium ring observed in DFT modelling. Additional signatures corresponding to B 1*s* and F 1*s* core levels reflect that [BF_4] anion remains electrostatically bound to the [BMIM] cation chemisorbed on the BP surface, as also observed through DFT studies (see Supplementary Fig. S9). The relative stability of pristine *vs* surface-passivated BP is also evident from XPS, which shows that while the pristine BP readily oxidises within 72 hours, the surface-treated BP remains largely stable. A marked decrease in the intensity of P–O feature in surface-treated BP confirms the ability of [BMIM][BF_4] in protecting BP against ambient degradation.

We next utilise confocal Raman spectroscopy to evaluate the ambient stability of the pristine and [BMIM][BF_4]-treated BP flakes (Fig. 3b). BP exhibits three distinct Raman modes at 361 cm^{-1} (A^1_g mode), 438 cm^{-1} (B^2_g mode) and 465 cm^{-1} (A^2_g mode). The A^1_g mode originates primarily from the out-of-plane vibrations of phosphorus atoms along the *c*-axis, while the B^2_g and A^2_g modes arise

from the in-plane vibrations of phosphorus atoms along the *b*-axis (armchair) and *a*-axis (zigzag), respectively.[27] The A^1_g mode is considered for the mapping as it remains constant when normalized to the Si transverse optical mode and hence provides a good reference for comparison.[28] In case of the pristine BP, the intensity of the A^1_g mode becomes non-existent within a week. However, the [BMIM][BF_4]-treated sample shows a largely non-variant intensity map even after 36 days of ambient storage and multiple cycles of exposure to a Raman laser. To quantify these observations, average peak intensities (normalised to the respective day 1 values) acquired on multiple flakes from each of the samples are analysed (Fig. 3c). It should be noted that this method of analysis does not fully take into account the severe reduction in lateral dimensions of pristine BP flakes due to rapid ambient deterioration. Nonetheless, all three Raman modes show an average reduction of up to 70% in the case of pristine BP (see Supplementary Fig. S10 for the analysis of the B^2_g and A^2_g modes), which remains an underestimation, considering the lateral size reduction. In contrast, the intensity average for the [BMIM][BF_4]-treated BP flakes, remains largely consistent, showing an intensity drop in the range of 7.5–9% over a period of 36 days. We attribute this drop to the laser induced photo-oxidation during multiple cycles of Raman spectral mapping. In fact, to circumvent this issue, an aluminium oxide passivating layer is typically deposited on BP flakes prior to extended Raman measurments, which is not required in our case. The average trend observed in multiple BP crystallites coupled with the spatial Raman analysis further highlights the effectivness of the proposed [BMIM][BF_4] RTIL-based surface treatment methodology against ambient degradation of BP.

To elucidate the applicability of our method to real world devices, we fabricate a field effect transistor (FET) from the [BMIM][BF_4]-treated BP. Figure 4a shows the *I-V* curves of a surface-treated BP FET at varying gate voltages. Figure 4b and 4c show a comparison of the transfer characteristics (I_{drain} *vs* V_{gate}) and transconductance obtained from a FET on a pristine and a [BMIM][BF_4]-treated BP flake, respectively. It is seen that the performance of the pristine sample

deteriorates rapidly within 8 days resulting in a total loss of switching properties. On the other hand, treatment with [BMIM][BF_4] preserves the electrical characteristics for 92 days.

Next we focus on understanding the mechanism responsible for protective effects of [BMIM][BF_4] RTIL. Recent studies have established that exposure of BP to light and molecular oxygen results in the generation of ROS.[29] These ROS have been assumed to play a dominant role in BP degradation,[3] as experimentally validated through our current ESEM studies. Analogously, in biological systems, natural antioxidants, such as carotenoids, play an important role in neutralising such damaging ROS.[4] More recently, artificial compounds such as imidazoles have also been found to sequester these damaging species.[30] As such, to understand the underlying role of [BMIM][BF_4] RTIL in BP protection, we investigate its influence on quenching three different ROS, namely, singlet oxygen species ($^1O_2$), as well as hydroxyl ($OH^{\cdot}$) and superoxide ($O_2^{\cdot -}$) radicals (Fig. 5) (see Supplementary Information for experimental details). A schematic depiction of the sequestration process is shown in Fig. 5a. It is seen from Fig. 5b that when photogenerated $^1O_2$ is exposed to as low as femtomolar concentrations of [BMIM][BF_4], this RTIL is able to sequester and quench ~90% of this damaging species. Other free radical species ($OH^{\cdot}$ and $O_2^{\cdot -}$) are also quenched, albeit requiring millimolar concentrations of RTIL to achieve similar degree of protection against photo-oxidation. Therefore, it is inferred that [BMIM][BF_4] provides a unique ability to protect BP via sequestering of the damaging ROS.

In summary, we demonstrate a robust biologically inspired procedure to stabilise BP and protect it from oxidation and deterioration, therefore transforming it to become amenable for device engineering. In particular, we first affirm the damaging role of ROS using an *in situ* ESEM study. Subsequently, we show that [BMIM][BF_4] RTIL has the ability to sequester these ROS, thereby preventing photo-oxidative degradation of mechanically exfoliated BP under ambient conditions. The chemical mechanism of the RTIL binding to BP is studied using DFT modelling. The surface-treated BP retains its key electronic characteristics for 92 days. This chemical sequestration strategy

offers new possibilities of employing chemo- and bio-molecules with antioxidant properties to protect environmentally-sensitive materials against photo-oxidative damages. Further investigations into this technique has the potential of achieving tunability of electronic/optoelectronic as well as chemical properties of BP, thereby having important implications for the field of 2D materials and systems.

Methods

Synthesis and treatment. For all the experiments conducted in this work, few-layer BP crystals were obtained via poly-dimethyl-siloxane (PDMS) assisted micromechanical exfoliation of commercial bulk black phosphorus crystals (Smart Elements) on a 50 nm SiO_2/Si substrate that were pre-cleaned using acetone and isopropanol and blow dried with N_2. Surface treatment was carried out straight after the synthesis process by drop-casting the RTILs on two separate samples. The RTILs were left on the surface for ~40 mins before being washed off using acetonitrile and blow dried with N_2.

Sample characterisation.

***In situ* SEM.** Electron beam irradiation was performed on pristine mechanically exfoliated few-layered BP on a SiO_2/Si substrate as well as RTIL-treated BP flakes. The samples were loaded in a variable pressure FEI Nova field emission gun SEM. The system was pumped down to a base pressure of $3x10^{-4}$ Pa. Water vapour was then injected into the chamber so as to achieve a chamber pressure of 8 Pa. The BP flakes were imaged using a magnetic-field-assisted gaseous secondary electron detector. Electron beam irradiation was performed by imaging the samples repeatedly with a 20 keV, 1.35 nA electron beam, using a scan rate of 3.36 ms/line and 1452 lines/frame. The flakes were exposed for up to three hours, as indicated in the figures.

Raman spectroscopy. The spatial Raman peak intensity mapping was conducted on a Horiba LabRam evolution micro Raman system equipped with 9 mW, 532 nm laser (0.5 μm lateral resolution, 0.25 sec exposure) and a 50× objective.

AFM. AFM imaging was conducted on a Dimension Icon AFM in Scan Assist mode.

ROS quenching studies. The ability of [BMIM][BF_4] RTIL to quench ROS was performed by assessing its impact on independently sequestering three oxidative species, namely $^1O_2$, O_2^- and $^{\cdot}OH$. These respective species were produced through photo-excitation of methylene blue, hypoxanthine/xanthine oxidase, and horseradish peroxidase, as elaborated in the supplementary information (Section 6).

BP FET fabrication and characterisation. FETs were fabricated on mechanically exfoliated BP on 50 nm SiO_2/Si substrates. After the transfer a photoresist was spin-coated at 4000 rpm for 45 sec followed by 100 ºC soft bake. The electrode patterns were UV exposed using a mask aligner system (MA6, SUSS MicroTech) and subsequently developed. The metal electrodes Cr/Au (10/100 nm) were then deposited on the developed using electron-beam metal deposition system. Finally, the lift-off in acetone was carried out to reveal the required metallic contact pads for micro-probes and electrical measurement. The FET measurements were conducted using a Keithley 4200SCS semiconductor parameter analyser. All measurements were performed under ambient conditions. The electrical characteristics were measured weekly for 36 days in parallel with the Raman measurements. Beyond that, the sample was left under ambient conditions and retested after 92 days.

References

1. Island JO, Steele GA, van der Zant HS, Castellanos-Gomez A. Environmental Instability of Few-Layer Black Phosphorus. *2D Materials*, **2**, 011002 (2015).
2. Wood JD, Wells SA, Jariwala D, Chen K-S, Cho E, Sangwan VK*, et al.* Effective Passivation of Exfoliated Black Phosphorus Transistors against Ambient Degradation. *Nano letters*, **14**, 6964-6970 (2014).

3. Favron A, Gaufrès E, Fossard F, Phaneuf-L'Heureux A-L, Tang NY, Lévesque PL*, et al.* Photooxidation and Quantum Confinement Effects in Exfoliated Black Phosphorus. *Nature materials*, **14**, 826-832 (2015).
4. Böhm F, Edge R, George Truscott T. Interactions of Dietary Carotenoids with Singlet Oxygen (1o2) and Free Radicals: Potential Effects for Human Health. *Acta Biochimica Polonica*, **59**, 27 (2012).
5. Tran V, Soklaski R, Liang Y, Yang L. Layer-Controlled Band Gap and Anisotropic Excitons in Few-Layer Black Phosphorus. *Physical Review B*, **89**, 235319 (2014).
6. Das S, Zhang W, Demarteau M, Hoffmann A, Dubey M, Roelofs A. Tunable Transport Gap in Phosphorene. *Nano letters*, **14**, 5733-5739 (2014).
7. Buscema M, Groenendijk DJ, Blanter SI, Steele GA, van der Zant HS, Castellanos-Gomez A. Fast and Broadband Photoresponse of Few-Layer Black Phosphorus Field-Effect Transistors. *Nano letters*, **14**, 3347-3352 (2014).
8. Liu H, Neal AT, Zhu Z, Luo Z, Xu X, Tománek D*, et al.* Phosphorene: An Unexplored 2d Semiconductor with a High Hole Mobility. *ACS nano*, **8**, 4033-4041 (2014).
9. Xia F, Wang H, Jia Y. Rediscovering Black Phosphorus as an Anisotropic Layered Material for Optoelectronics and Electronics. *Nature communications*, **5**, (2014).
10. Chen Y, Ren R, Pu H, Chang J, Mao S, Chen J. Field-Effect Transistor Biosensors with Two-Dimensional Black Phosphorus Nanosheets. *Biosensors and Bioelectronics*(2016).
11. Dai J, Zeng XC. Bilayer Phosphorene: Effect of Stacking Order on Bandgap and Its Potential Applications in Thin-Film Solar Cells. *The journal of physical chemistry letters*, **5**, 1289-1293 (2014).
12. Li W, Yang Y, Zhang G, Zhang Y-W. Ultrafast and Directional Diffusion of Lithium in Phosphorene for High-Performance Lithium-Ion Battery. *Nano letters*, **15**, 1691-1697 (2015).
13. Rahman MZ, Kwong CW, Davey K, Qiao SZ. 2d Phosphorene as a Water Splitting Photocatalyst: Fundamentals to Applications. *Energy & Environmental Science*, **9**, 709-728 (2016).
14. Yasaei P, Behranginia A, Foroozan T, Asadi M, Kim K, Khalili-Araghi F*, et al.* Stable and Selective Humidity Sensing Using Stacked Black Phosphorus Flakes. *ACS nano*, **9**, 9898-9905 (2015).
15. Kou L, Chen C, Smith SC. Phosphorene: Fabrication, Properties, and Applications. *The journal of physical chemistry letters*, **6**, 2794-2805 (2015).
16. Kim J-S, Liu Y, Zhu W, Kim S, Wu D, Tao L*, et al.* Toward Air-Stable Multilayer Phosphorene Thin-Films and Transistors. *Scientific Reports*, **5**, 8989 (2015).
17. Barber J, Andersson B. Too Much of a Good Thing: Light Can Be Bad for Photosynthesis. *Trends in biochemical sciences*, **17**, 61-66 (1992).
18. Xie C, Zhang X, Wu Y, Zhang X, Zhang X, Wang Y*, et al.* Surface Passivation and Band Engineering: A Way toward High Efficiency Graphene–Planar Si Solar Cells. *Journal of Materials Chemistry A*, **1**, 8567-8574 (2013).
19. Aberle AG. Surface Passivation of Crystalline Silicon Solar Cells: A Review. *Progress in Photovoltaics: Research and Applications*, **8**, 473-487 (2000).
20. Shen J, Zhu Y, Yang X, Zong J, Zhang J, Li C. One-Pot Hydrothermal Synthesis of Graphene Quantum Dots Surface-Passivated by Polyethylene Glycol and Their Photoelectric Conversion under near-Infrared Light. *New Journal of Chemistry*, **36**, 97-101 (2012).
21. Wang J. Carbon-Nanotube Based Electrochemical Biosensors: A Review. *Electroanalysis*, **17**, 7-14 (2005).
22. Zhang J, Liu X, Blume R, Zhang A, Schlögl R, Su DS. Surface-Modified Carbon Nanotubes Catalyze Oxidative Dehydrogenation of N-Butane. *Science*, **322**, 73-77 (2008).
23. Ryder CR, Wood JD, Wells SA, Yang Y, Jariwala D, Marks TJ*, et al.* Covalent Functionalization and Passivation of Exfoliated Black Phosphorus Via Aryl Diazonium Chemistry. *Nature chemistry*(2016).
24. Zhao Y, Wang H, Huang H, Xiao Q, Xu Y, Guo Z*, et al.* Surface Coordination of Black Phosphorus for Robust Air and Water Stability. *Angewandte Chemie*, **128**, 5087-5091 (2016).
25. Martin AA, Bahm A, Bishop J, Aharonovich I, Toth M. Dynamic Pattern Formation in Electron-Beam-Induced Etching. *Physical review letters*, **115**, 255501 (2015).

26. Edmonds M, Tadich A, Carvalho A, Ziletti A, O'Donnell K, Koenig S*, et al.* Creating a Stable Oxide at the Surface of Black Phosphorus. *ACS applied materials & interfaces*, **7**, 14557-14562 (2015).
27. Łapińska A, Taube A, Judek J, Zdrojek M. Temperature Evolution of Phonon Properties in Few-Layer Black Phosphorus. *The Journal of Physical Chemistry C*, **120**, 5265-5270 (2016).
28. Zhang S, Yang J, Xu R, Wang F, Li W, Ghufran M*, et al.* Extraordinary Photoluminescence and Strong Temperature/Angle-Dependent Raman Responses in Few-Layer Phosphorene. *Acs Nano*, **8**, 9590-9596 (2014).
29. Wang H, Yang X, Shao W, Chen S, Xie J, Zhang X*, et al.* Ultrathin Black Phosphorus Nanosheets for Efficient Singlet Oxygen Generation. *Journal of the American Chemical Society*, **137**, 11376-11382 (2015).
30. Zhao L, Zhang C, Zhuo L, Zhang Y, Ying JY. Imidazolium Salts: A Mild Reducing and Antioxidative Reagent. *Journal of the American Chemical Society*, **130**, 12586-12587 (2008).

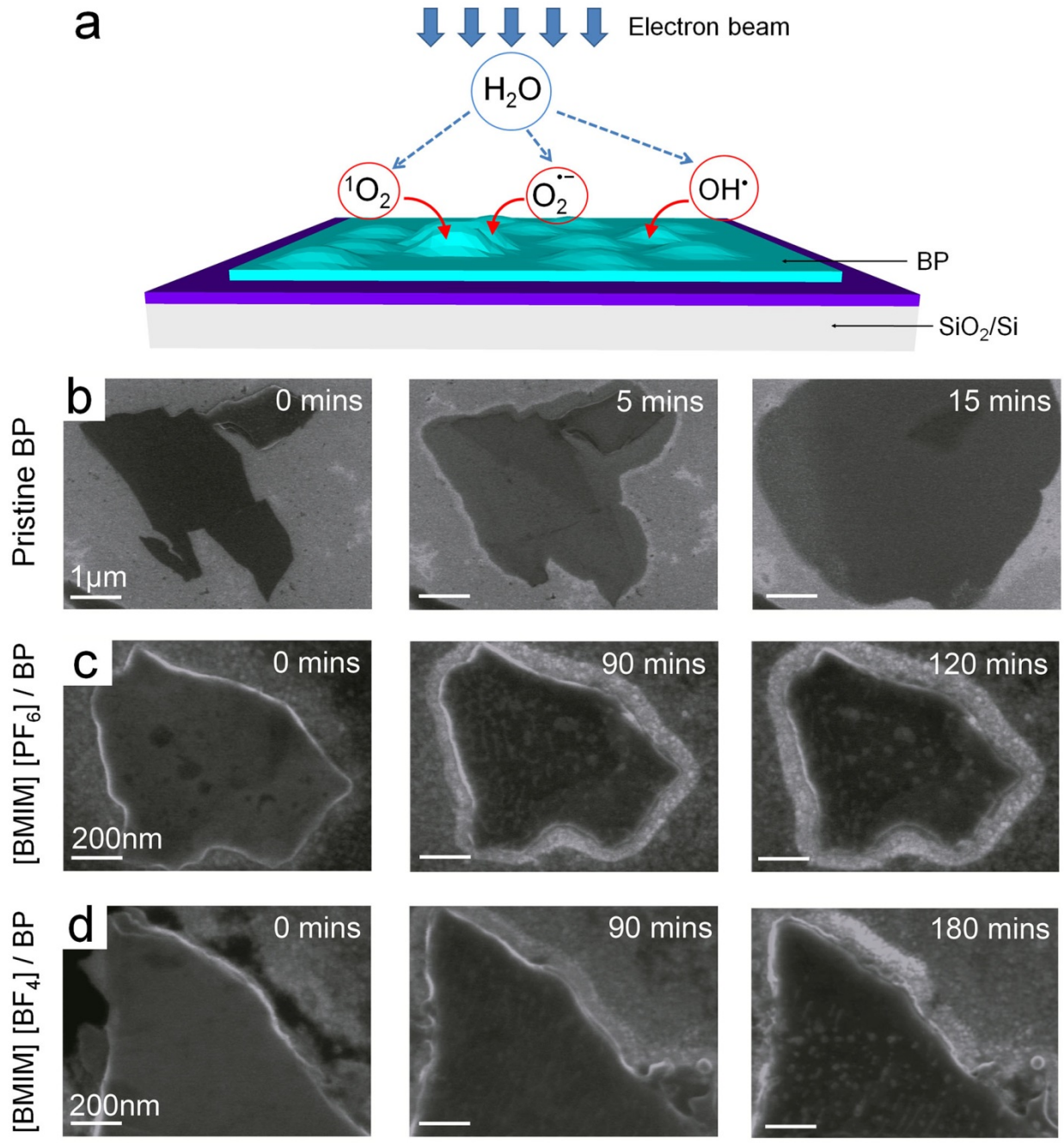

Figure 1| *In situ* SEM study of BP degradation via ROS Production. a, Schematic representation of the electron beam induced ROS production that causes degradation of an unprotected BP surface. **b-d,** SEM micrographs of the BP flakes imaged in the presence of H_2O vapour **a,** pristine BP. **b,** [BMIM][PF_6]-treated BP and **c,** [BMIM][BF_4]-treated BP flakes. The

flake in (a) deteriorated and shrunk rapidly into the small dark feature as seen in the figure, as well as in Supplementary Video 1.

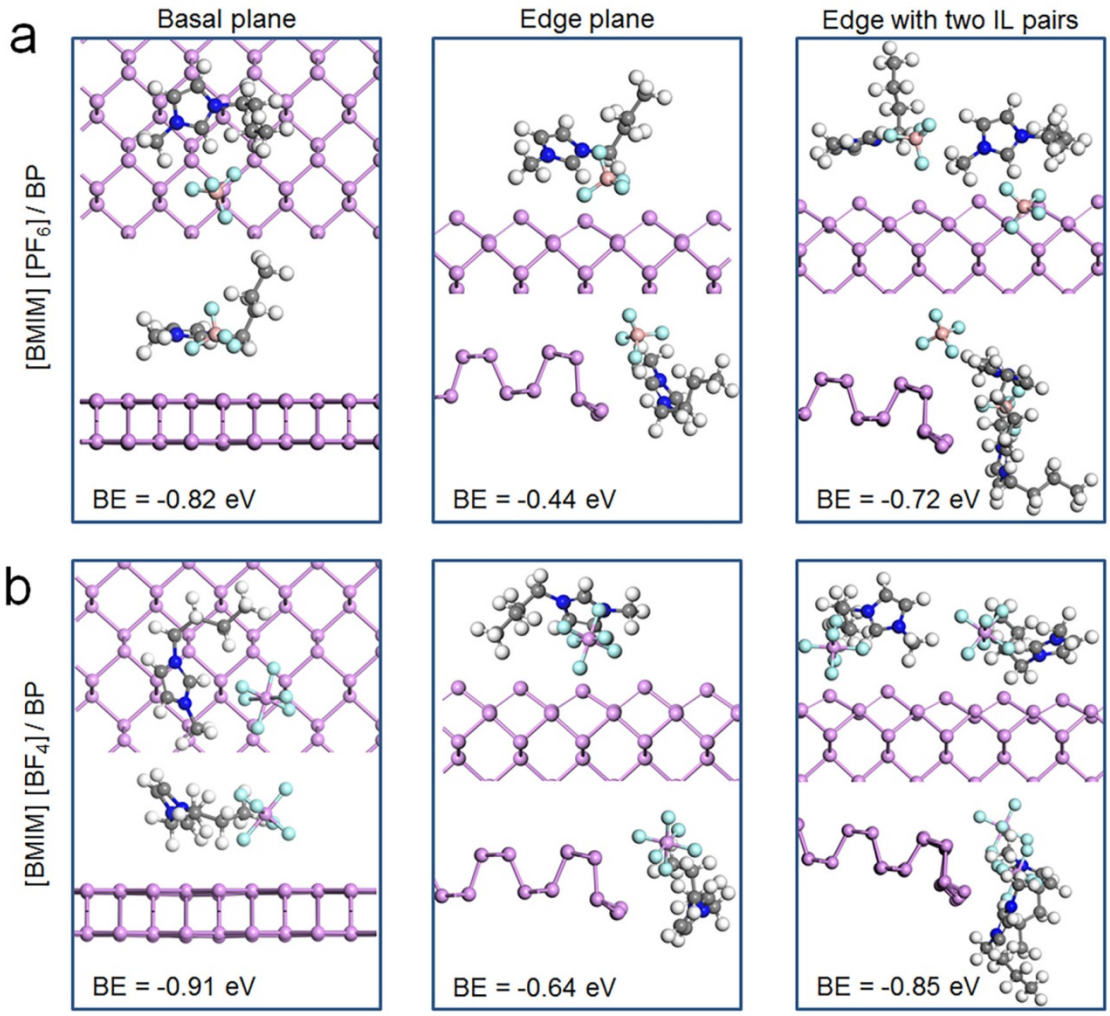

Figure 2| DFT modelling of RTIL-treated BP. (Left to right) DFT-calculated thermodynamically favoured structures and corresponding binding energies for RTILs **a,** [BMIM][PF_6] and **b,** [BMIM][BF_4] adsorption on BP basal plane, edge plane and with two RTIL pairs on the edge plane. It is evident that the [BMIM][BF_4] binds more strongly to both BP planes compared to [BMIM][PF_6].

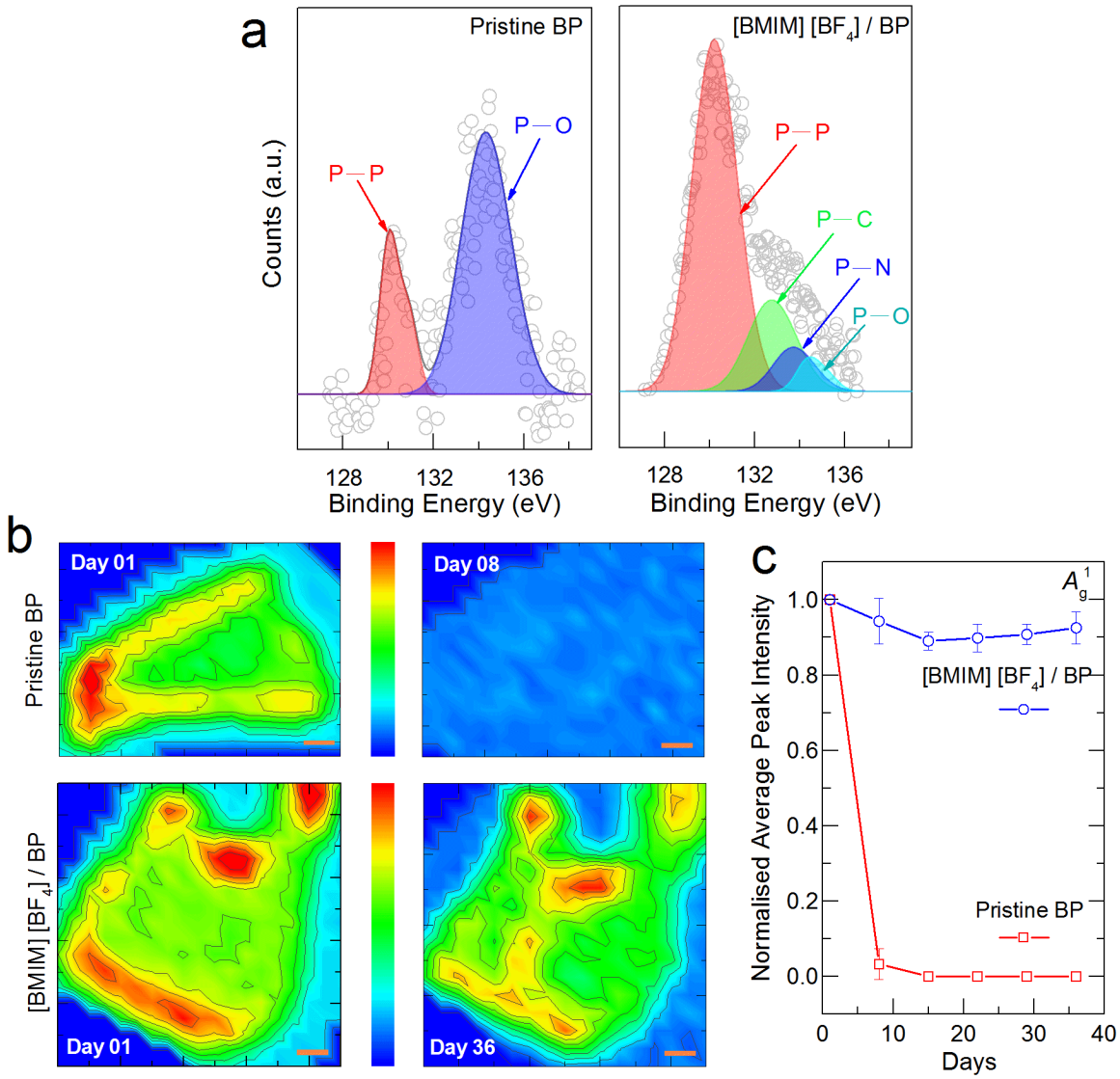

Figure 3| Spectroscopic characterization of BP. **a,** Deconvoluted P 2*p* core-level XPS spectra after 72 hours of ambient exposure for a pristine and a [BMIM][BF_4]-treated BP flake. The evolution of the P–O feature at 134.1 eV in pristine BP is indicative of the photo-oxidation at the surface within 72 hours. In the case of a surface-treated BP flake, the P–P, P–C and P–N features are predominant. **b,** Spatial Raman peak intensity maps (A^1_g) for a representative pristine BP (Day 01 and 08) and [BMIM][BF_4]-treated BP flake (Day 01 and 36). Scale bars denote 1 µm. **c,** Evolution of the normalised intensity (averaged from multiple BP flakes) of the A^1_g Raman mode over the course of ambient exposure. It can be seen that even after multiple exposures to the Raman

laser, the surface-treated flakes are largely preserved. The error bars represent a confidence interval of 95%.

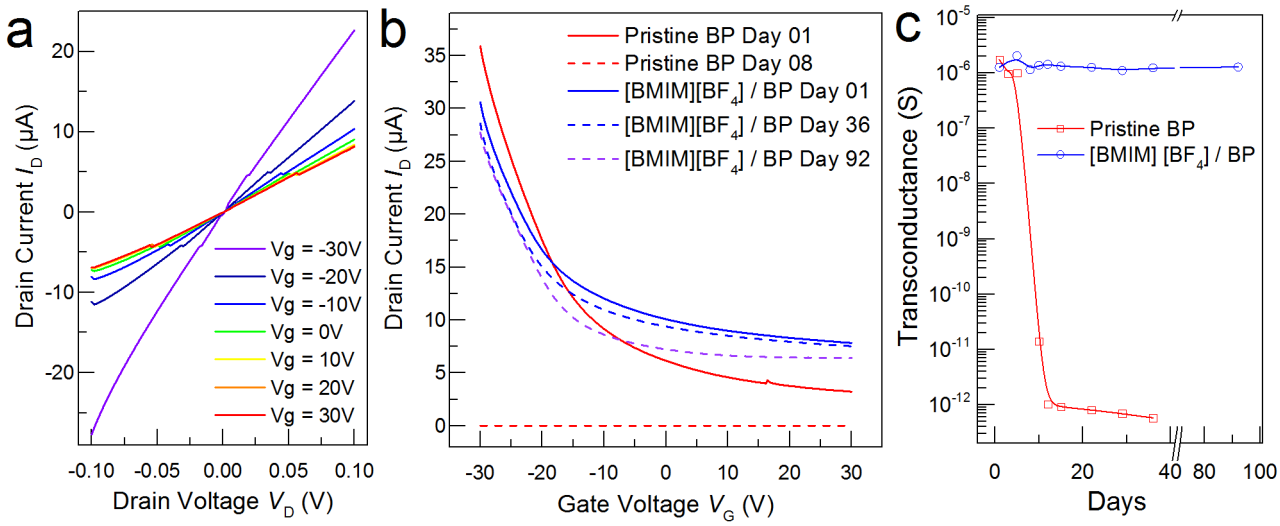

Figure 4| FET characteristics of an untreated and [BMIM][BF_4]-treated BP flake. a, *I-V* curves of a [BMIM][BF_4]-treated BP FET with varying gate voltages. **b,** Transfer characteristics of a pristine and [BMIM][BF_4]-treated BP FET over the course of ambient exposure. **c,** comparison of transconductance of a pristine and [BMIM][BF_4]-treated BP FET over 92 days. It is seen that the characteristics of surface-treated BP FETs are preserved, whereas the electronic properties of the pristine BP FET shows rapid degradation within 8 days.

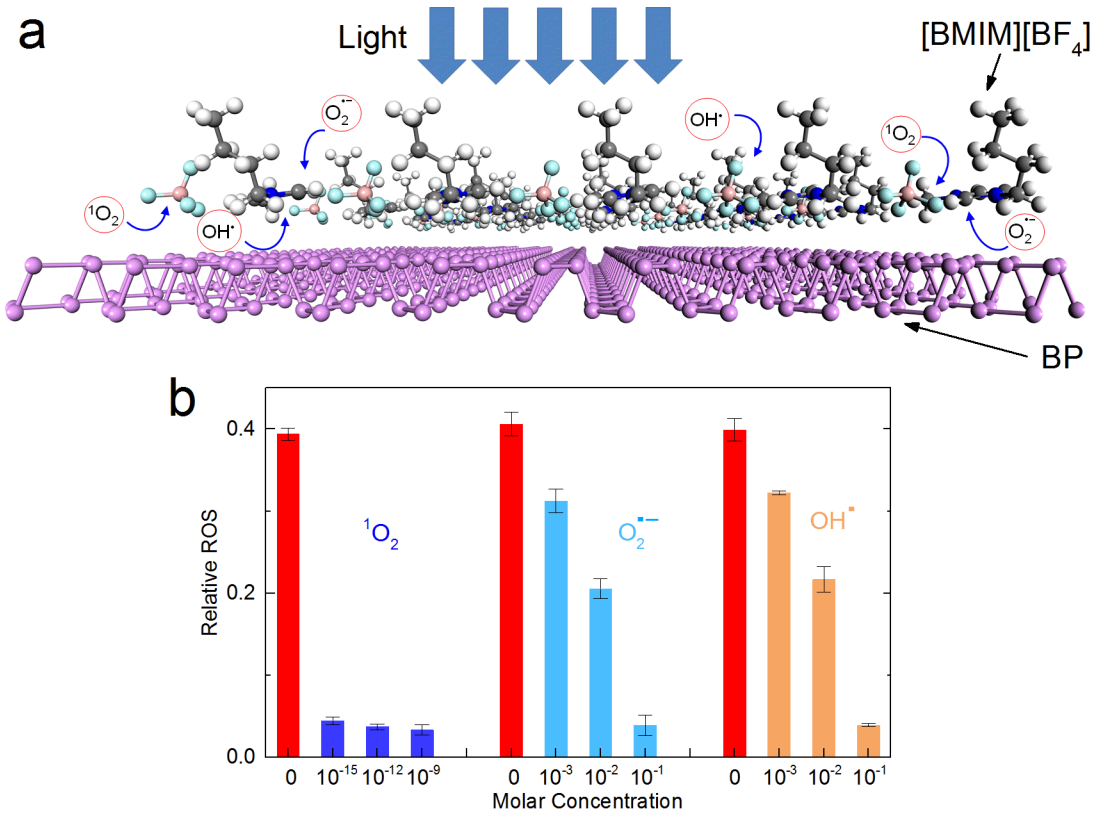

Figure 5| Protection of BP through [BMIM][BF_4]-mediated ROS sequestration. a, A schematic representation of the ROS sequestration via [BMIM][BF_4] RTIL on the BP surface **b,** The ability of [BMIM][BF_4] to quench different photo-oxidative species, wherein the differences in the molar concentrations of the RTIL required to quench $^1O_2$, OH· and $O_2^{\bullet-}$ levels are notable.